FRI-TEM: Time Encoding Sampling of Finite-Rate-of-Innovation Signals

Hila Naaman, *Student Member, IEEE*, Satish Mulleti, *Member, IEEE*, and Yonina C. Eldar, *Fellow, IEEE*

***Abstract*—Classical sampling is based on acquiring signal amplitudes at specific points in time, with the minimal sampling rate dictated by the degrees of freedom in the signal. The samplers in this framework are controlled by a global clock that operates at a rate greater than or equal to the minimal sampling rate. At high sampling rates, clocks are power-consuming and prone to electromagnetic interference. An integrate-and-fire time encoding machine (IF-TEM) is an alternative power-efficient sampling mechanism which does not require a global clock. Here, the samples are irregularly spaced threshold-based samples. In this paper, we investigate the problem of sampling FRI signals using an IF-TEM. We provide theoretical guarantees for a recently proposed recovery method to perfectly recover an FRI input. In addition, we propose a modified sampling approach in the presence of noise that is more robust than existing techniques. This method is also proven to ensure recovery in the noise-free setting. The modified approach requires twice the number of measurements compared to the existing method, however, it results in lower error in the presence of noise for the same number of measurements. Our results enable designing low-cost and energy-efficient analog-to-digital converters for FRI signals.**

***Index Terms*—Time-encoding machine (TEM), finite-rate-of-innovation (FRI) signals, time-based sampling, integrate and fire TEM (IF-TEM), sub-Nyquist sampling, analog-to-digital conversion, non-uniform sampling.**

I. Introduction

SAMPLING is a process which enables discrete representation of continuous-time signals allowing for efficient processing of analog signals using digital signal processors [1], [2]. A commonly used discrete representation is to measure uniform, instantaneous samples of an analog signal, as in Shannon-Nyquist sampling theory [3], and more general shift-invariant sampling [4], [5]. The amplitude samples are measured via a sample and hold circuit that is controlled by a global clock that operates at a speed greater or equal to the minimum sampling rate. At high sampling rates, clocks are power consuming and subject to electromagnetic interference [6].

Time encoding machines (TEM) provide an alternative digital representation of analog signals [7]–[14], which is asynchronous, that is, no global clock is required unlike conventional analog to digital converters. This leads to lower power consumption and reduced electromagnetic interference [6]. In this sampling scheme, an analog signal is represented by a set of time instants at which the input signal or its function crosses a certain threshold. The number of time instants per unit time or *firing rate* is proportional to the local frequency content of the input signal. For example, there are more firings in a region where the signal amplitude varies rapidly compared to regions with relatively slow variations.

A popular approach for time encoding is an integrate and fire time encoding machine (IF-TEM), which is a brain-inspired sampling paradigm. It leads to simple and energy-efficient devices, such as analog-to-digital converters [9], [11], neuromorphic computers [15], event-based vision sensors [16], and more. In an IF-TEM, a bias is added to the analog input to make the signal positive. The resulting signal is then scaled and integrated, and the integral value is compared to a threshold. Each time the threshold is reached, time points or firing instants are recorded, which encode the information of the analog signal [7], [17]. A natural question is whether the analog input can be perfectly reconstructed from the time-encodings.

In recent years time-based sampling theory has witnessed growing interest with several authors proving the capabilities of TEM to sample and reconstruct bandlimited signals [8], [13], [17]–[20], [20]. Interestingly, the minimum firing rate of a TEM for perfect recovery of a bandlimited signal is equal to the Nyquist rate of the signal. Since the firing rate has to increase with bandwidth, we look beyond the bandlimited structure of the signal so that sampling can be performed at a sub-Nyquist rate.

In the sub-Nyquist regime, finite-rate-of-innovation (FRI) signals are widely studied [1], [21], [22]. These signals have fewer degrees of freedom than the signal's Nyquist rate, which enables sub-Nyquist sampling [23]. As an example, consider an FRI signal consisting of a sum of L amplitude-scaled and time-delayed copies of a known pulse. Since the pulse is known, the signal is completely specified by L amplitudes and L time-delays, which amounts to $2L$ degrees of freedom. It has been shown that $2L$ measurements of the signal uniquely determine the amplitude and the time-delays. A typical FRI sampling scheme is shown in Fig. 1 where the signal is first filtered by a sampling kernel to remove redundancy in the signal, and then

Manuscript received June 9, 2021; revised October 11, 2021, November 24, 2021, and March 28, 2022; accepted April 8, 2022. Date of publication April 18, 2022; date of current version May 16, 2022. The associate editor coordinating the review of this manuscript and approving it for publication was Prof. Jarvis Haupt. This work was supported in part by the Israeli Council for Higher Education through the Weizmann Data Science Research Center, in part by a research grant from the Estate of Tully and Michele Plesser, in part by the European Union's Horizon 2020 Research and Innovation Program under Grant 646804-ERC-COG-BNYQ, in part by Israel Science Foundation under Grant 0100101, and in part by the QuantERA under Grant C'MON-QSENS. *(Hila Naaman and Satish Mulleti contributed equally to this work.) (Corresponding author: Hila Naaman.)*

Hila Naaman and Yonina C. Eldar are with the Faculty of Math and Computer Science, Weizmann Institute of Science, Rehovot 76100, Israel (e-mail: hilanaaman10@gmail.com; yonina.eldar@weizmann.ac.il).

Satish Mulleti is with the Department of Electrical Engineering, Indian Institute of Technology Bombay, Mumbai 400076, India (e-mail: mulleti.satish@gmail.com).

Digital Object Identifier 10.1109/TSP.2022.3167146

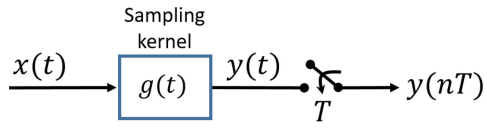

Fig. 1. A kernel-based FRI sampling framework: An FRI signal $x(t)$ is first filtered by a sampling kernel $g(t)$ and then instantaneous uniform samples are measured at a sub-Nyquist rate. Parameters of the FRI signal are estimated from the sub-Nyquist samples.

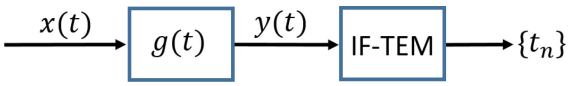

Fig. 2. Sampling setup: A continuous-time signal $x(t)$ is filtered through a sampling kernel $g(t)$ and then sampled by a TEM which generates time-instants $\{t_n\}$.

instantaneous samples are measured at a sub-Nyquist rate [22]. Given the advantage of TEM over conventional sampling, we are interested in studying the applicability of TEM-based sampling to FRI signals.

We consider the TEM-based sampling scheme for FRI signals shown in Fig. 2, where the signal is modeled as a sum of shifted and scaled pulses with a known pulse shape. Our goal is to develop conditions on the sampling kernel and IF-TEM parameters so that perfect recovery is guaranteed.

Alexandru and Dragotti [10] consider a sequential reconstruction method for certain FRI signals. They show that by using either a compactly supported polynomial generating kernel or an exponential generating kernel, the time delays and amplitudes of each pulse can be perfectly recovered from four firing instants. Thus, to reconstruct a stream of L pulses with $2L$ degrees of freedom, $4L$ firing instants are needed. The sequential nature of the reconstruction imposes a restriction on the minimum separation between any two consecutive pulses, such that any two successive pulses must be separated by the support of the sampling kernel. In addition, the threshold of the IF-TEM must be small enough to achieve a sufficient firing rate. To address these issues, Hilton *et al.* [11] consider IF-TEM sampling by using the derivative of a hyperbolic secant as a sampling kernel. They showed that a stream of L Dirac impulses or piecewise constant functions with L discontinuities are perfectly reconstructed from $3L + 1$ firing instants without any minimum separation conditions. However, the sampling mechanism can not be extended to FRI signals with arbitrary known pulse shapes.

Rudresh *et al.* [12] show that by using sampling kernels that have a frequency-domain alias cancellation properties (see [22] for details), FRI signals with $2L$ degrees of freedom can be recovered from $2L + 2$ IF-TEM firing instants. The reconstruction algorithm does not require any minimum separation conditions but assumes that certain invertibility conditions are guaranteed. Through simulations, the authors show that the invertibility conditions are satisfied for a large number of experiments; however, theoretical guarantees are not provided. In addition, their sampling results do not deal with the noisy scenario.

Our contribution is twofold. First, we derive theoretical guarantees for perfect reconstruction of FRI signals with arbitrary but known pulse shapes using the method in [12]. Second, we design a sampling kernel and IF-TEM sampler with improved noise robustness compared to existing techniques by modifying the approach in [12]. Specifically, since FRI signals with $2L$ degrees of freedom can be perfectly reconstructed from $2L$ consecutive Fourier series coefficients (FSCs) [1], [22], we choose sampling kernels with the alias-cancellation condition to annihilate the undesirable FSCs [22]. The filtered signal, with fewer FSCs, is applied to an IF-TEM, and firing instants are measured. We show that $2L + 2$ firing instants are sufficient to uniquely determined $2L$ FSCs from which the original signals can be recovered. Furthermore, we establish conditions on the IF-TEM parameters that ensure that the minimum firing rate is achieved. To summarize, we show that by using a sampling kernel with frequency-domain alias-cancellation properties and an IF-TEM sampler with a minimum firing rate of $2L + 2$ per time unit, an FRI signal with $2L$ degrees of freedom is uniquely recovered.

While the above sampling approach leads to perfect reconstruction of the signal in the absence of noise, the reconstruction can be highly sensitive to noise as we show in simulations. To address this issue, we propose a modified sampling and reconstruction mechanism. In particular, we show that the zeroth Fourier coefficient of the filtered signal results in an unstable inverse while computing the FSCs from the time instants in the presence of noise. To improve noise robustness we modify the sampling kernel by removing the zero-frequency component. For this modified method, we show that $4L + 2$ time instants are sufficient for perfect recovery when the time-delays of the FRI signal are off-grid, whereas $2L + 2$ firings are sufficient when the delays are on grid.

Through simulations, we show that for the same number of firing rates (beyond $2L + 2$ firings), the mean squared error in the estimation of the on-grid time delays in the proposed approach is 2–6 dB lower compared to the one in [12]. In the case of off-grid time delays, we consider perturbations in the time encoding. We show that the proposed approach has more than 3–10 dB gain in terms of error compared to the method in [12] for the same number of measurements. In addition, we also show that the proposed approach has better resolution ability in the presence of noise. Specifically, when the FRI pulses are close to each other, the proposed method is able to distinguish them.

This paper is organized as follows. In Section II-A we review IF-TEM, followed by a problem formulation in Section II-B. In Section III, we present our first recovery result where the sampling kernel includes a zero-frequency component. A noise-robust sampling and reconstruction method together with simulations are presented in Section IV. In Section V, we discuss recovery guarantees for non-periodic FRI signals. Concluding remarks are presented in Section VI.

II. Problem Formulation and Preliminaries

We begin by presenting some known results on IF-TEM followed by the problem formulation.

A. Time Encoding Machine

We consider an IF-TEM whose operating principle is the same as in [17] (except that the refractory period is assumed to be zero, see Fig. 3). The input to the IF-TEM is a bounded signal $y(t)$, and the output is a series of firing or time instants. An IF-TEM is parametrized by positive real numbers b, κ, and δ and works

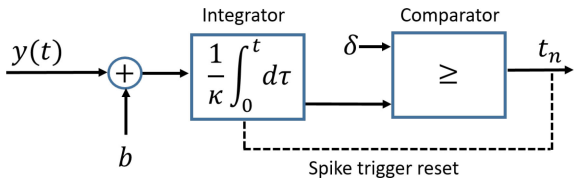

Fig. 3. Time encoding machine with spike trigger reset. The input is biased by b, scaled by κ, and integrated. A time instant is recorded when the threshold δ is reached, after which the value of the integrator resets.

as follows: A bias b is added to a c-bounded signal $y(t)$ where $|y(t)| \leq c < b < \infty$, and the sum is integrated and scaled by κ. When the resulting signal reaches the threshold δ, the time instant t_n is recorded, and the integrator is reset. The process is repeated to record subsequent time instants, i.e., if a time instant t_n was recorded, the next time instant t_{n+1} satisfies

$$\frac{1}{\kappa}\int_{t_n}^{t_{n+1}} (y(s)+b)\,ds = \delta. \tag{1}$$

The time encodings $\{t_n, n \in \mathbb{Z}\}$ form a discrete representation of the analog signal $y(t)$ and the objective is to reconstruct $y(t)$ from them. Typically, reconstruction is performed by using an alternative set of discrete representations $\{y_n, n \in \mathbb{Z}\}$ defined as

$$y_n \triangleq \int_{t_n}^{t_{n+1}} y(s)\,ds = -b(t_{n+1}-t_n) + \kappa\delta. \tag{2}$$

The measurements $\{y_n, n \in \mathbb{Z}\}$ are derived from the time encodings $\{t_n, n \in \mathbb{Z}\}$ and IF-TEM parameters $\{b, \kappa, \delta\}$.

Although reconstruction methods vary for different classes of signals, for perfect recovery of any signal, the firing rate is required to satisfy a lower bound that depends on the degrees of freedom of the signal. The firing rate of an IF-TEM is bounded both from above and below, where the bounds are a function of the IF-TEM parameters and an upper-bound on the signal amplitude. Using (2) and the fact that $|y(t)| \leq c$, it can be shown that for any two consecutive time instants [17], [18]:

$$\frac{\kappa\delta}{b+c} \leq t_{n+1}-t_n \leq \frac{\kappa\delta}{b-c}. \tag{3}$$

The inequalities in (3) imply that in any arbitrary, non-zero, observation interval T_{obs}, the maximum and minimum number of firings are

$$T_{\text{obs}}\frac{b+c}{\kappa\delta} \quad \text{and} \quad T_{\text{obs}}\frac{b-c}{\kappa\delta}, \tag{4}$$

respectively. Thus, the firing rate of an IF-TEM F_R with parameters b, κ, and δ are upper and lower bounded as

$$\frac{b-c}{\kappa\delta} \leq F_R \leq \frac{b+c}{\kappa\delta}. \tag{5}$$

Our goal is to recover a continuous-time FRI signal $x(t)$ of the form of (6) below, from the time instances $\{t_n\}$.

B. Problem Formulation

We consider a T-periodic FRI signal of the form

$$x(t) = \sum_{p\in\mathbb{Z}}\sum_{\ell=1}^{L} a_\ell h(t-\tau_\ell - pT), \tag{6}$$

where $h(t)$ is a known, real-valued pulse and the amplitudes and delays $\{(a_\ell,\tau_\ell)|\tau_\ell \in [0,T), a_\ell \in (0, a_{\max}]\}_{\ell=1}^{L}$ are unknown parameters. This signal model is ubiquitous in applications such as radar [24]–[26], ultrasound [22], [27], and more. In these applications, $h(t)$ denotes a known transmit pulse which is reflected from L targets. The reflected signal is modeled as $x(t)$ where a_ℓ and τ_ℓ denote the amplitude and time-delay corresponding to the ℓ-th target.

In general, FRI signals can have wide bandwidth due to short duration pulses $h(t)$. However, by using the structure of the signal and knowledge of the pulse $h(t)$, FRI signals can be sampled at sub-Nyquist rates. This is typically achieved by passing $x(t)$ through a designed sampling kernel $g(t)$ and then measuring low-rate samples of the filtered signal $y(t)$ as shown in Fig. 1. The kernel is designed such that the FRI parameters $\{a_\ell,\tau_\ell\}_{\ell=1}^{L}$ are computed accurately from the samples. In particular, it has been shown that $2L$ samples of $y(t)$ in an interval of length T, that are measured either uniformly [21], [22] or non-uniformly [28], [29], are sufficient to determine $\{a_\ell,\tau_\ell\}_{\ell=1}^{L}$ uniquely. The reconstruction or determination of the parameters from the samples is achieved by applying spectral analysis methods such as the annihilating filter [1], [21].

As discussed in the introduction, a conventional FRI sampling scheme, such as in Fig. 1, has a sampler which is controlled by a global clock that operates at the rate of innovation $\frac{2L}{T}$ Hz. For a large L or a small T, the sampling rate increases, and the global clock requires high power. In this case, an IF-TEM sampler is well suited as it does not require a global clock.

We consider the problem of perfect recovery of the FRI parameters $\{a_\ell,\tau_\ell\}_{\ell=1}^{L}$ using an IF-TEM sampling scheme as shown in Fig. 2. Specifically, we consider designing the sampling kernel $g(t)$ and an IF-TEM such that the FRI parameters are uniquely determined from the time-encodings by keeping the firing rate close to the rate of innovation.

In the next section, we follow a similar strategy to the one in [12], and show that in the noiseless case, perfect recovery is guaranteed using as few as $2L+2$ firings in an interval of length T. In Section IV-A, we suggest an alternative approach that is more robust to noise.

III. FRI-TEM: Sampling and Perfect Recovery of FRI Signals From IF-TEM Measurements

In this section, we show that FRI signals can be perfectly recovered from IF-TEM measurements. We use the fact that the FRI signal $x(t)$ in (6) can be perfectly reconstructed from its $2L$ FSCs. We derive conditions on the IF-TEM parameters and the sampling kernel $g(t)$ such that $2L$ FSCs of the input FRI signal can be uniquely recovered from the IF-TEM output. Our approach is similar to the one considered in [12]. However, in contrast to [12], we mathematically derive exact recovery guarantees.

A. Fourier-Series Representation of FRI Signals

We begin by explicitly relating the input signal $x(t)$ of (6) to its FSCs (cf. (10)) following [22].

Since $x(t)$ is a T-periodic signal, it has a Fourier series representation

$$x(t) = \sum_{k\in\mathbb{Z}} \hat{x}[k]e^{jk\omega_0 t}, \tag{7}$$

where $\omega_0 = \frac{2\pi}{T}$. The Fourier-series coefficients $\hat{x}[k]$ are given by

$$\hat{x}[k] = \frac{1}{T}\hat{h}(k\omega_0)\sum_{\ell=1}^{L} a_\ell e^{-jk\omega_0\tau_\ell}, \tag{8}$$

where, $\hat{h}(\omega)$ is the continuous-time Fourier transform of $h(t)$ and we assume that $\hat{h}(k\omega_0) \neq 0$ for $k \in \mathcal{K}$ where $\mathcal{K}$ is a given set of indices. Since $x(t)$ is real-valued, its FSCs $\hat{x}[k]$ are complex conjugate pairs, that is,

$$\hat{x}^*[-k] = \hat{x}[k]. \tag{9}$$

The sequence

$$\frac{\hat{x}[k]}{\hat{h}(k\omega_0)} = \frac{1}{T}\sum_{\ell=1}^{L} a_\ell e^{-jk\omega_0\tau_\ell}, \tag{10}$$

consists of a sum of L complex exponentials. From the theory of high-resolution spectral estimation [30], it is well known that $2L$ consecutive samples of $\frac{\hat{x}[k]}{\hat{h}(k\omega_0)}$ are sufficient to determine $\{a_\ell, \tau_\ell\}_{\ell=1}^{L}$. For example, one can apply the well known annihilating filter method [21] to compute $\{a_\ell, \tau_\ell\}_{\ell=1}^{L}$. In practice, the pulse $h(t)$ has short-duration and wide bandwidth. Hence, there always exist $2L$ or more non-vanishing Fourier samples $\hat{h}(k\omega_0)$ that are computed a priori. To determine the FRI parameters, we need to compute $2L$ consecutive values of $\hat{x}[k]$. Our problem is then reduced to that of uniquely determining the desired number of FSCs from the signal measurements. Since $x(t)$ typically consists of a large number of FSCs, we discuss next a sampling kernel design which removes unnecessary FSCs and thus reduces the sampling rate.

B. Sampling Kernel

Since a minimum of $2L$ FSCs are sufficient for uniquely recovering the FRI signal, the sampling kernel $g(t)$ is designed to remove or annihilate any additional FSCs. The filtered signal $y(t)$ is given by

$$\begin{aligned} y(t) = (x * g)(t) &= \int_{-\infty}^{\infty} x(\tau) g(t-\tau) d\tau \\ &= \sum_{k\in\mathbb{Z}} \hat{x}[k] \int_{-\infty}^{\infty} g(t-\tau) e^{jk\omega_0\tau} d\tau \\ &= \sum_{k\in\mathbb{Z}} \hat{x}[k]\, \hat{g}(k\omega_o)\, e^{jk\omega_0 t}. \end{aligned} \tag{11}$$

To restrict the summation to a finite number of terms and annihilate the unwanted FSCs we define the filter to satisfy the following condition in the Fourier domain:

$$\hat{g}(k\omega_0) = \begin{cases} 1 & \text{if } k \in \mathcal{K}, \\ 0 & \text{otherwise}, \end{cases} \tag{12}$$

where $\mathcal{K}$ is a set of integers such that $|\mathcal{K}| \geq 2L$.

One particular choice of the sampling kernel is a sum-of-sincs (SoS) kernel [22] generated by

$$\hat{g}(\omega) = \sum_{k\in\mathcal{K}} \operatorname{sinc}\left(\frac{\omega}{\omega_0} - k\right), \tag{13}$$

and

$$g(t) = \begin{cases} \sum_{k\in\mathcal{K}} e^{jk\omega_0 t}, & t \in (-T/2, T/2] \\ 0, & \text{elsewhere.} \end{cases} \tag{14}$$

The sampling kernel $g(t)$ is designed to pass the coefficients $\hat{x}[k], k \in \mathcal{K}$ while suppressing all other coefficients $\hat{x}[k], k \notin \mathcal{K}$. Note that one can also apply an ideal lowpass filter with appropriate cutoff frequency to remove the FSCs. However, the impulse response of an ideal lowpass filter has infinite support, whereas the SoS kernel has compact support.

Using a SoS kernel, the filtered signal $y(t)$ is

$$y(t) = \sum_{k\in\mathcal{K}} \hat{x}[k]\hat{g}(k\omega_0)e^{jk\omega_0 t} = \sum_{k\in\mathcal{K}} \hat{x}[k]e^{jk\omega_0 t}. \tag{15}$$

The filtered signal $y(t)$ is sampled by an IF-TEM which requires its input to be real-valued and bounded. Since $\hat{x}[k]$ are conjugate symmetric, to ensure that $y(t)$ is real valued, the support set $\mathcal{K}$ is chosen to be symmetric around zero, that is, $\mathcal{K}$ is given as

$$\mathcal{K} = \{-K, \ldots, K\}, \tag{16}$$

where $K \geq L$ to ensure that there are at-least $2L$ FSCs of $x(t)$ retained in $y(t)$.

From (6) and $y(t) = (x * g)(t)$, it can be shown that

$$c \triangleq \max_t |y(t)| \leq L\ a_{\max}\ \|(h * g)\|_\infty \tag{17}$$

$$\leq L\ a_{\max}\ \|g\|_\infty \|h\|_1, \tag{18}$$

where Young's convolution inequality is used. Since $|g(t)| \leq |\mathcal{K}|$ and $\mathcal{K}$ is a finite set, $g(t)$ is bounded. Hence $y(t)$ is bounded provided that the maximal amplitude $a_{\max} < \infty$ and the pulse $h(t)$ is absolutely integrable. In the remaining of the paper, we assume that both these conditions hold.

C. FRI TEM Sampling

The IF-TEM input is the filtered signal $y(t)$, which is the T-periodic signal defined in (15). The output of the IF-TEM is a set of time instants $\{t_n\}_{n\in\mathbb{Z}}$. Given $\{t_n\}$ one can determine the measurements $\{y_n\}$ by using (2). The relation between the measurements y_n and the desired FSCs is given by [12]

$$\begin{aligned} y_n &= \int_{t_n}^{t_{n+1}} y(t)\, dt \\ &= \int_{t_n}^{t_{n+1}} \sum_{k\in\mathcal{K}\setminus\{0\}} \hat{x}[k]e^{jk\omega_0 t} dt + \int_{t_n}^{t_{n+1}} \hat{x}[0] dt \\ &= \sum_{k\in\mathcal{K}\setminus\{0\}} \hat{x}[k] \frac{\left(e^{jk\omega_0 t_{n+1}} - e^{jk\omega_0 t_n}\right)}{jk\omega_0} + \hat{x}[0]\,(t_{n+1} - t_n)\,. \end{aligned} \tag{20}$$

To extract the desired FSCs from (20), we denote by $\mathbf{y}$ the vector $[\int_{t_1}^{t_2} y(t)dt, \int_{t_2}^{t_3} y(t)dt, \ldots, \int_{t_{N-1}}^{t_N} y(t)dt]^\top$, where N is the number of time instants in the interval T, and let

$$\hat{\mathbf{x}} = \left[-\frac{\hat{x}[-K]}{jK\omega_0}, \ldots, \hat{x}[0], \ldots, \frac{\hat{x}[K]}{jK\omega_0}\right]^\top. \tag{21}$$

With this notation, (20) can be written in the following matrix form:

$$\mathbf{y} = \mathbf{A}\hat{\mathbf{x}}, \tag{22}$$

where $\mathbf{A}$ be given in (19). This equation describes the relation between the IF-TEM measurements and the FSCs. Our goal is to determine these FSCs embedded in $\hat{\mathbf{x}}$ from which we can perfectly recover the FRI parameters. If the matrix $\mathbf{A}$ has full column rank then the Fourier coefficients vector can be computed as

$$\hat{\mathbf{x}} = \mathbf{A}^{\dagger}\mathbf{y}, \tag{23}$$

where $\mathbf{A}^{\dagger}$ denotes the Moore-Penrose inverse.

In [12], the matrix is assumed to be uniquely left-invertible. The authors showed via simulations that the matrix has full column rank, however, a proof is not presented. In the following we show that for an adequate number of firings, the matrix $\mathbf{A}$ is indeed uniquely left-invertible, that is, has full column rank.

D. Recovery Guarantees

In this section, we present our main results where we show that for the sampling kernel choice (14), we can uniquely identify the FSCs from the IF-TEM time instants. Specifically, we show that for a particular choice of the IF-TEM parameters, the matrix $\mathbf{A}$ defined in (19) is left invertible. Our results are summarized in the following theorems.

Theorem 1: Consider a positive integer K and a number $T > 0$. Let $0 \leq t_1 < t_2 < \cdots < t_N < T$ for an integer N, and $\omega_0 = \frac{2\pi}{T}$. Then the matrix $\mathbf{A}$ defined in (19) is left-invertible provided that $N \geq 2K + 2$.

Proof: See the Appendix. □

Theorem 1 implies that there should be a minimum of $2K + 2$ IF-TEM time instants within an interval of T to enable recovery of the FSCs, and subsequent reconstruction of the FRI signal. To ensure this, the minimum firing rate $\frac{b-c}{\kappa\delta}$ (cf. (5)) should be chosen such that

$$\frac{b-c}{\kappa\delta} \geq \frac{2K+2}{T}. \tag{24}$$

By combining Theorem 1, the result in (24), and the fact that $2L$ FSCs are sufficient to recover the FRI parameters, we summarize the sampling and reconstruction of FRI signals using IF-TEM in the following theorem.

Theorem 2: Let $x(t)$ be a T-periodic FRI signal of the following form

$$x(t) = \sum_{p\in\mathbb{Z}} \sum_{\ell=1}^{L} a_\ell h(t - \tau_\ell - pT),$$

where $\tau_\ell \in [0, T)$, $|a_\ell| < \infty$, and L is known. We assume that the amplitudes $\{a_\ell\}_{\ell=1}^{L}$ are finite, and the pulse $h(t)$ is known and absolutely integrable. Consider the sampling mechanism shown in Fig. 2. Let the sampling kernel $g(t)$ satisfy

$$\hat{g}(k\omega_0) = \begin{cases} 1 & \text{if } k \in \mathcal{K} = \{-K, \ldots, K\}, \\ 0 & \text{otherwise,} \end{cases}$$

and $\max_t |(h * g)(t)| < \infty$. Choose the real positive TEM parameters $\{b, \kappa, \delta\}$ such that $c < b < \infty$, where c is defined in (18), and

$$\frac{b-c}{\kappa\delta} \geq \frac{2K+2}{T}. \tag{25}$$

Then, the parameters $\{a_\ell, \tau_\ell\}_{\ell=1}^{L}$ can be perfectly recovered from the TEM outputs if $K \geq L$.

Based on Theorem 2, a reconstruction algorithm to compute the FRI parameters from TEM firings is presented in Algorithm 1.

TABLE I
IF-TEM PARAMETERS CHOICE FOR ESTIMATION

L	b	δ	κ	ω_0	F_R (samples/s)
3	0.9	0.07	1	2π	13
5	1.3	0.07	1	2π	18
10	2.5	0.07	1	2π	36

E. IF-TEM Parameter Selection

The IF-TEM parameters are selected such that there is a minimum of $N \geq 2L + 2$ time instants $\{t_n\}_{n=1}^{N}$ within a time interval T. Thus, the minimum firing rate that enables accurate reconstruction is $\frac{2L+2}{T}$. The maximum firing rate is bounded by $\frac{b+c}{\kappa\delta}$. While the threshold δ, which is a parameter of the comparator, is easier to control, the integrator constant κ is a parameter of the integrator, and it is usually fixed. Thus, assuming a fixed value of b and κ, choosing small δ results in a large firing rate above the minimum desirable value of $\frac{2L+2}{T}$. In practice, both b and δ are generated through a DC voltage source, and therefore large values of bias and threshold require high power. Hence, to minimize the power requirements, it is desirable for b and δ to be as small as possible.

F. Simulations

We next numerically validate Theorem 2. In Fig. 4, we consider $h(t)$ as a Dirac impulse with time period $T = 1$ seconds. We consider the simulations for $L = 3$, 5, and 10. The time delays and amplitudes are selected uniformly at random over $(0, 1)$. The input signal $x(t)$ is filtered using an SoS sampling kernel with $\mathcal{K} = \{-K, \ldots, K\}$, where $K = L$. The filtered output $y(t)$ is sampled using an IF-TEM which has a threshold $\delta = 0.07$ and $\kappa = 1$. The bias of the IF-TEM is set as $b = 0.9$, 1.3, and 2.5 for $L = 3$, 5, and 10 respectively. The parameters are chosen to satisfy the inequality in (25), and resulted in 13, 18, and 36 samples per period for $L = 3$, 5, and 10. As per Theorem 2, 8, 12, and 22 samples per period are sufficient. The reconstruction was found to be stable even for a larger number of impulses. We summarize the choice of IF-TEM parameters and the resulting firing rate in Table I. In Fig. 5, using the

$$\mathbf{A} = \begin{bmatrix} e^{-jK\omega_0 t_2} - e^{-jK\omega_0 t_1} & \cdots & t_2 - t_1 & \cdots & e^{jK\omega_0 t_2} - e^{jK\omega_0 t_1} \\ e^{-jK\omega_0 t_3} - e^{-jK\omega_0 t_2} & \cdots & t_3 - t_2 & \cdots & e^{jK\omega_0 t_3} - e^{jK\omega_0 t_2} \\ \vdots & & \vdots & & \vdots \\ e^{-jK\omega_0 t_N} - e^{-jK\omega_0 t_{N-1}} & \cdots & t_N - t_{N-1} & \cdots & e^{jK\omega_0 t_N} - e^{jK\omega_0 t_{N-1}} \end{bmatrix}. \tag{19}$$

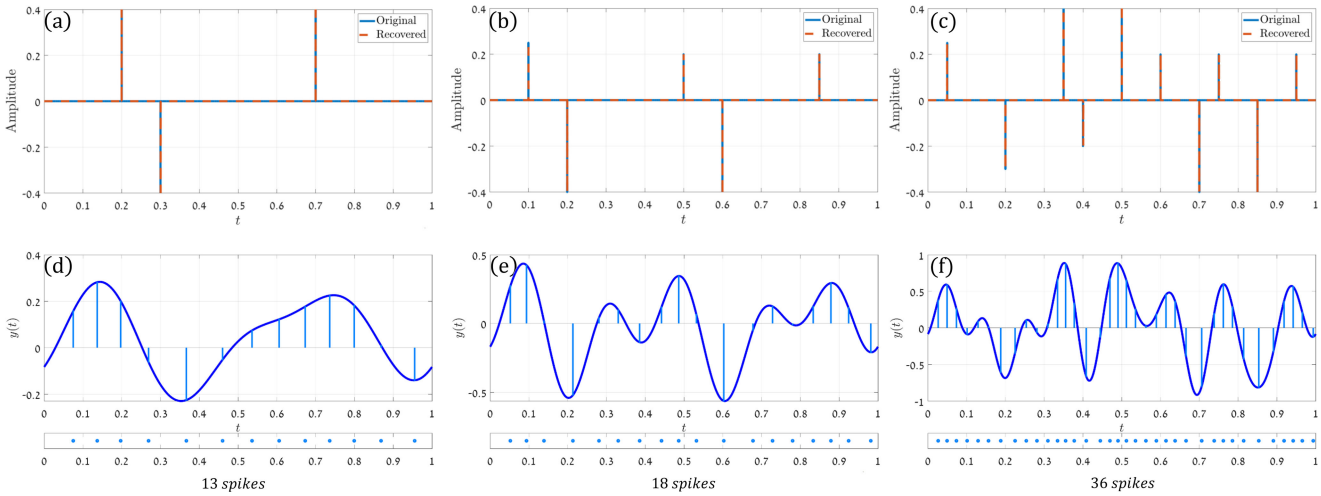

Fig. 4. Sampling and reconstruction of a stream of Dirac impulses using TEM by applying the SoS kernel. Both τ_ℓ and a_ℓ are chosen uniformly at random over $(0, 1)$. (a)–(c): the input signal and its reconstruction for $L = 3$, $L = 5$, and $L = 10$ respectively. (d)–(f): the filtered signal $y(t)$ and the time instants t_n for $L = 3$, $L = 5$, and $L = 10$ respectively.

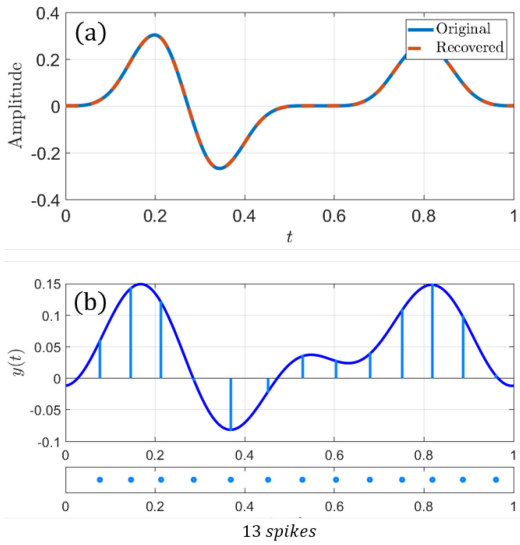

Fig. 5. Sampling and reconstruction of stream of pulses using TEM by applying the SoS kernel. (a): the input signal and its reconstruction for $L = 3$. (b): the filtered signal $y(t)$ and the time instants t_n for $L = 3$.

same filter, we depict the estimation of a stream of pulses with $L = 3$, $\{a_\ell\} = \{0.5, -0.45, 0.4\}$, and $\{\tau_\ell\} = \{0.2, 0.33, 0.8\}$. The IF-TEM b, δ, κ which satisfy the inequality in (25), are 0.9,0.07,1 respectively. The resulting firing rate is as few as 13 samples/s.

IV. Noise Robustness

The results in [12] and the previous section assume that there is no measurement noise. However, in practice, the signals are contaminated by noise. In the presence of noise, the IF-TEM outputs or time instants are perturbed. While using Algorithm 1, this results in a perturbation in the matrix $\mathbf{A}$ as well as the measurements $\mathbf{y}$ in (22). In this case, when computing the FSCs using (22), the stability of $\mathbf{A}$, which is measured by the condition number of the matrix, impacts the results. Next, we show that

Algorithm 1: Reconstruction of a T-Periodic FRI Signal Using Theorem 2.

Input: $N \geq 2K + 2$ spike times $\{t_n\}_{n=1}^N$ in a period T.

1: Let $n \leftarrow 1$
2: **while** $n \leq N - 1$ **do**
3: Compute $y_n = -b(t_{n+1} - t_n) + \kappa\delta$
4: $n := n + 1$.
5: **end while**
6: Compute Fourier coefficients vector $\hat{\mathbf{x}} = \mathbf{A}^\dagger \mathbf{y}$ in (23).
7: Estimate $\{(a_\ell, \tau_\ell)\}_{\ell=1}^L$ using a spectral analysis method.

Output: $\{(a_\ell, \tau_\ell)\}_{\ell=1}^L$.

by excluding zero from $\mathcal{K}$, perfect recovery is possible, and in the noisy scenario, the resulting method is more robust.

As we show below, when excluding the zero vector, we end up with a recovery problem similar to (23) but with the matrix $\mathbf{B}$ defined in (29) replacing $\mathbf{A}$. This matrix has better condition number than $\mathbf{A}$. To gain intuition as to why this is the case, we consider the intersection of a function $f(t)$ and a straight line $r(t)$ as shown in Fig. 6. The function $f(t)$ is a K-th order trigonometric polynomial whose coefficients are FSCs of the FRI signal and the slope of $r(t)$ is equal to $\bar{x}[0] = \hat{x}[0]$ (see the Appendix for more details). As we discuss in detail in the Appendix, the closer the values of $f(t)$ to $r(t)$ at the time encoding instants, the poorer the condition number of the corresponding matrices.

As shown in the Appendix, the matrices $\mathbf{A}$ and $\mathbf{B}$ have full column rank provided that the straight line $r(t) \neq f(t)$ at all time encoding instants $\{t_n\}_{n=1}^N$, and this condition holds for $N > 2K + 1$. Note that $\bar{x}[0] \neq 0$ when we consider matrix $\mathbf{A}$ and $\bar{x}[0] = 0$ in the context of matrix $\mathbf{B}$. Furthermore, we can show that the smaller the values of $\{|r(t) - f(t)|\}_{t_n=1}^N$ the poorer the condition number. For $N > 2K + 1$ and $\bar{x}[0] \neq 0$, it is possible that there exists a set of time encodings $\{t_n\}_{n=1}^N$ such that the straight line $r(t)$ is close to the trigonometric polynomial $f(t)$

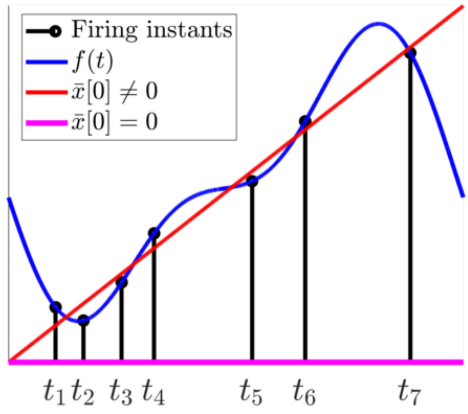

(a) Condition numbers of $\mathbf{A}$ is 30 and of $\mathbf{B}$ is 3

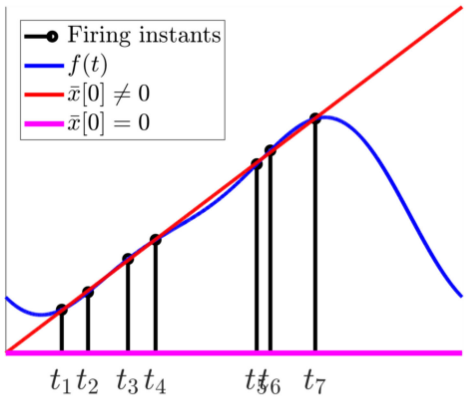

(b) Condition numbers of $\mathbf{A}$ is 3000 and of $\mathbf{B}$ is 5

Fig. 6. Examples $f(t)$ and $r(t)$ when the matrix $\mathbf{A}$ has large condition number.

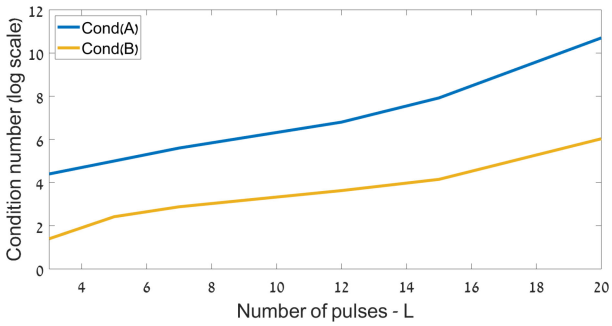

Fig. 7. Average condition number of matrices $\mathbf{A}$ and $\mathbf{B}$ as a function of L.

at $\{t_n\}_{n=1}^N$. In such a case, from (44), we can determine a set of Fourier coefficients such that $\mathbf{A}\hat{\mathbf{x}} \approx \mathbf{0}_N$, where $\mathbf{0}_N$ is a zero vector of length N. Hence for that particular set of $\{t_n\}_{n=1}^N$, $\mathbf{A}$ becomes ill-conditioned. However, when $\bar{x}[0] = 0$, we observe that it is less likely that $r(t)$ with zero-slope becomes close to $f(t)$ at the time-encoding instants. Several illustrative examples depicting this intuition are shown in Fig. 6 where $K = 2$ and $N = 7$. In Fig. 6(a), the condition number of matrices $\mathbf{A}$ and $\mathbf{B}$ are 30 and 3, respectively. The condition number of $\mathbf{A}$ is ten times higher than that of $\mathbf{B}$. This is because the straight line corresponding to $\mathbf{A}$ (shown in red) is closer to the trigonometric polynomial at the time-encodings than that of $\mathbf{B}$ (in magenta). In the example shown in Fig. 6(b), the condition number of $\mathbf{A}$ is 3000 as $|r(t) - f(t)|$ is small for $t \in \{t_n\}_{n=1}^N$, whereas $|r(t) - f(t)|$ is relatively large for $\bar{x}[0] = 0$ and consequently $\mathbf{B}$ has lower condition number.

Next, we present a perfect recovery guarantee for FRI signals by using IF-TEM without the zero frequency in the SoS kernel.

A. Exclusion of Zero

In this section, we show that by excluding the zero frequency in $\mathcal{K}$ we achieve perfect reconstruction for FRI signals of the form of (6). In this case, the resulting matrix has a much more stable structure compared to $\mathbf{A}$ of (19).

Suppose we remove $k = 0$ following (20), we have

$$\begin{aligned} y_n &= \int_{t_n}^{t_{n+1}} y(t)\, dt \\ &= \int_{t_n}^{t_{n+1}} \sum_{k\in\mathcal{K}\setminus\{0\}} \hat{x}[k] e^{jk\omega_0 t} dt \\ &= \sum_{k\in\mathcal{K}\setminus\{0\}} \hat{x}[k] \frac{\left(e^{jk\omega_0 t_{n+1}} - e^{jk\omega_0 t_n}\right)}{jk\omega_0}. \end{aligned} \tag{26}$$

To extract the FSCs from (26), we denote by $\mathbf{y}_0$ the vector $[\int_{t_1}^{t_2} y(t)dt, \int_{t_2}^{t_3} y(t)dt, \ldots, \int_{t_{N-1}}^{t_N} y(t)dt]^\top$, where N is the number of time instants in the interval T. The measurements $\mathbf{y}_0$ and the FSCs

$$\hat{\mathbf{x}}_0 = \left[-\frac{\hat{x}[-K]}{jK\omega_0}, \ldots, -\frac{\hat{x}[-1]}{j\omega_0}, \frac{\hat{x}[1]}{j\omega_0}, \ldots, \frac{\hat{x}[K]}{jK\omega_0}\right]^\top \tag{27}$$

are now related as

$$\mathbf{y}_0 = \mathbf{B}\hat{\mathbf{x}}_0, \tag{28}$$

where $\mathbf{B}$ is given as in (29). Next, we show that the matrix $\mathbf{B}$ has full column rank and is uniquely left invertible (29) shown at the bottom of next page.

Theorem 3: Consider a positive integer K and a number $T > 0$. Let $0 \leq t_1 < t_2 < \cdots < t_N < T$ for an integer N, and $\omega_0 = \frac{2\pi}{T}$. Then the matrix $\mathbf{B}$ defined in (29) is left-invertible provided that $N > 2K + 1$.

Proof: The proof follows the same line as that of Theorem 1 with the constraint $\hat{x}[0] = 0$ as detailed in Case-1 in the Appendix. □

Since the left-inverse of $\mathbf{B}$ exists, the Fourier coefficients vector is computed as

$$\hat{\mathbf{x}}_0 = \mathbf{B}^\dagger \mathbf{y}_0. \tag{30}$$

Although, the FSCs are computed uniquely, they are not consecutive unlike the FSCs computed in Theorem 2. Since high resolution spectral estimation techniques such as the annihilating filter requires $2L$ consecutive FSCs, to uniquely determine the FRI parameters, we need $K \geq 2L$. This results in twice the firing rate compared to that in Theorem 2. An alternative approach to reduce the firing rate is to assume that the time-delays are on a grid. In this case, determination of time-delays and amplitudes of the FRI signal from FSCs is cast as a compressive sensing problem [24, Section V-B]. This problem is efficiently solved from $2L$ FSCs, that are not necessarily consecutive, by using sparse recovery approaches such as orthogonal matching pursuit (OMP) [1, Ch. 11]. Hence, by assuming that the time-delays of the FRI signal are on a grid, we require $K \geq L$.

Algorithm 2: Reconstruction of a T-Periodic FRI Signal.

Input: $N \geq 2K+2$ spike times $\{t_n\}_{n=1}^{N}$ in a period T.
1: Let $n \leftarrow 1$
2: **while** $n \leq N-1$ **do**
3: Compute $y_n = -b(t_{n+1} - t_n) + \kappa\delta$
4: $n := n+1$.
5: **end while**
6: Compute Fourier coefficients vector $\hat{\mathbf{x}}_0 = \mathbf{B}^{\dagger}\,\mathbf{y_0}$ in (30).
7: Estimate $\{(a_\ell, \tau_\ell)\}_{\ell=1}^{L}$ from $\hat{\mathbf{x}}_0$ by using CS methods for $K \geq L$.
Output: $\{(a_\ell, \tau_\ell)\}_{\ell=1}^{L}$.

The minimum firing rate for the IF-TEM is

$$\frac{b-c}{\kappa\delta} \geq \frac{2K+2}{T}, \tag{31}$$

where $K \geq 2L$ for off-grid time-delays and $K \geq L$ for time-delays on-grid. By combining Theorem 3 with the result in (31), we summarize the sampling and reconstruction of FRI signals using IF-TEM in the following theorem.

Theorem 4: Let $x(t)$ be a T-periodic FRI signal of the following form

$$x(t) = \sum_{p\in\mathbb{Z}} \sum_{\ell=1}^{L} a_\ell h(t - \tau_\ell - pT),$$

where the number of FRI signals L is known, and $h(t)$ is a signal with known pulse shape. Consider the sampling mechanism shown in Fig. 2. Let the sampling kernel $g(t)$ satisfy

$$\hat{g}(k\omega_0) = \begin{cases} 1 & \text{if } k \in \mathcal{K} = \{-K, \ldots, -1, 1, \ldots, K\}, \\ 0 & \text{otherwise,} \end{cases}$$

and $\max_t |(h * g)(t)| < \infty$. Choose the real positive TEM parameters $\{b, \kappa, \delta\}$ such that $c < b < \infty$, where c is defined in (18), and

$$\frac{b-c}{\kappa\delta} \geq \frac{2K+2}{T}. \tag{32}$$

Then, the parameters $\{a_\ell, \tau_\ell\}_{\ell=1}^{L}$ can be perfectly recovered from the TEM outputs if

1) $K \geq 2L$ when $\{\tau_\ell\}_{\ell=1}^{L}$ are off-grid
2) $K \geq L$ when $\{\tau_\ell\}_{\ell=1}^{L}$ are on-grid.

Since the time delays and amplitudes of the FRI signals are estimated uniquely, without any constant offset, from any set of $2L$ or more consecutive FSCs, excluding the zero frequency does not result in any offset in the reconstruction. An algorithm to perfectly recover the FRI parameters from IF-TEM samples is summarized in Algorithm 2.

B. Numerical Results for On-Grid Time-Delays

In many practical systems, the time instants can only be recorded with finite precision, i.e., in practical circumstances, the recorded times are effective time instances $\{t'_n\}$ which differ from the real-time instances $\{t_n\}$, and perfect reconstruction may no longer be possible [10], [31].

We compare the robustness of the Algorithms 1 and 2 in the presence of perturbation to the measured time instants. We demonstrate that Algorithm 2 provides better recovery than Algorithm 1.

In the above Algorithms, the first step is to estimate the Fourier samples from the TEM measurements by taking pseudo inverses of $\mathbf{A}$ (cf. (22)) and $\mathbf{B}$ (cf. (28)), respectively. Both the matrices are functions of the measured time instants and the sampling kernel. In Fig. 7, we compare the condition numbers of the matrices with perturbed firing instants as a function of the number of FRI signals L. To that aim, 5000 random sets of monotonic sequences $\{t_n \in [0, T)\}_{n=1}^{N}$ were used. As shown in Fig. 7, the condition number of the matrix $\mathbf{B} \in \mathbb{C}^{(4L+2)\times(2L)}$ is substantially smaller than the condition number of the matrix $\mathbf{A} \in \mathbb{C}^{(4L+2)\times(2L+1)}$.

Next, we illustrate the reconstruction of a T-periodic FRI signal from non-uniform noisy samples (time instants) using the two reconstruction algorithms of Theorems 2 and 4. We created a periodic FRI signal $x(t)$ of the form of (6). The signal $x(t)$ with period $T = 1$ consists of $L = 3$ pulses with $h(t) = \beta^{(3)}(20t)$, where $\beta^{(3)}(t)$ is a third-order cubic B-spline, with $\{a_\ell\}_{\ell=1}^{3} = \{0.5, -0.45, 0.4\}$, and $\{\tau_\ell\}_{\ell=1}^{3} = \{0.2, 0.4, 0.8\}$. The TEM parameters are $b = 1.2$, $\kappa = 1$, and δ changes from 0.04 to 0.09 resulting in 13 to 24 time samples. The parameters are chosen to satisfy condition (32). We consider a sum-of-sincs kernel with $\mathcal{K} = \{-K, \ldots, 0, \ldots, K\}$ for Theorem 2, and $\mathcal{K} = \{-K, \ldots, -1, 1, \ldots, K\}$ for Theorem 4. For both kernels, the time instances $\{t_n\}$ were perturbed by a zero-mean white Gaussian noise with variance 0.001. For both the methods we set $K = 2L$ and applied OMP to recover the time-delays and amplitudes [1].

The reconstruction accuracy of the two algorithms is compared in terms of relative mean square error (MSE), given by

$$\text{MSE} = \frac{||x(t) - \bar{x}(t)||_{L_2[0,T]}}{||x(t)||_{L_2[0,T]}}, \tag{33}$$

where $\bar{x}(t)$ is the reconstructed signal. In Fig. 8, we show the MSE of the two algorithms as a function of the number of noisy time instances. The MSE of Algorithm 2 is 2–6 dB lower compared to that of Algorithm 1 for different firing rates.

Next, we compare the two frameworks when the input FRI signal has noise. To simulate a continuous-time noise effect on the input to IF-TEM, we add perturbation to the FSCs at the output of the SoS filter. In the noisy case, the output of the SoS

$$\mathbf{B} = \begin{bmatrix} e^{-jK\omega_0 t_2} - e^{-jK\omega_0 t_1} & \ldots & e^{-j\omega_0 t_2} - e^{-j\omega_0 t_1} & e^{j\omega_0 t_2} - e^{j\omega_0 t_1} & \ldots & e^{jK\omega_0 t_2} - e^{jK\omega_0 t_1} \\ e^{-jK\omega_0 t_3} - e^{-jK\omega_0 t_2} & \ldots & e^{-j\omega_0 t_3} - e^{-j\omega_0 t_2} & e^{j\omega_0 t_3} - e^{j\omega_0 t_2} & \ldots & e^{jK\omega_0 t_3} - e^{jK\omega_0 t_2} \\ \vdots & & \vdots & \vdots & & \vdots \\ e^{-jK\omega_0 t_N} - e^{-jK\omega_0 t_{N-1}} & \ldots & e^{-j\omega_0 t_N} - e^{-j\omega_0 t_{N-1}} & e^{j\omega_0 t_N} - e^{j\omega_0 t_{N-1}} & \ldots & e^{jK\omega_0 t_N} - e^{jK\omega_0 t_{N-1}} \end{bmatrix} \tag{29}$$

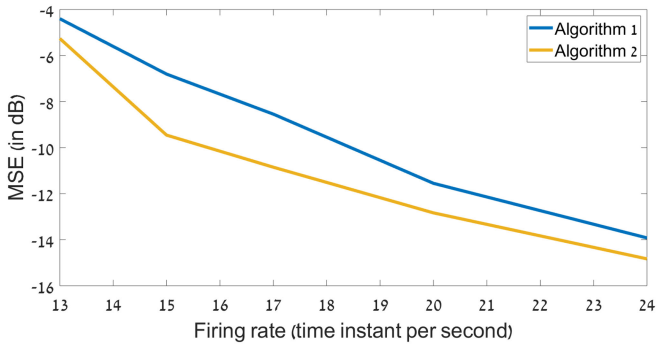

Fig. 8. Performance comparison of Algorithm 1 and Algorithm 2 in the presence of continuous-time white Gaussian noise with zero mean and variance 0.001.

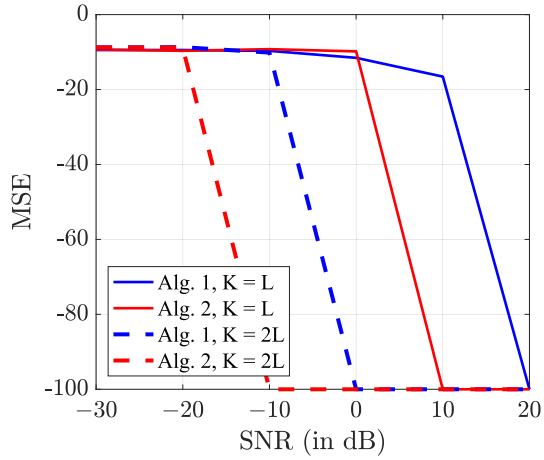

Fig. 9. A comparison of Algorithm 1 and Algorithm 2 with noisy input signal: For SNR> -20 dB, Algorithm 2 has lower error compared to Algorithm 1.

filter is given by

$$y'(t) = \sum_{k\in\mathcal{K}} \left(\hat{x}[k] + \xi[k]\right) e^{jk\omega_0 t}, \tag{34}$$

where $\{\xi[k]\}_{k\in\mathcal{K}}$ are independent and identically distributed circular complex Gaussian random variables with zero mean and variance $\sigma_{\hat{x}}$. In this simulation, we define SNR as

$$10\log_{10}\left(\frac{\sum_{k\in\mathcal{K}}|\hat{x}[k]|^2}{|\mathcal{K}|\sigma_{\hat{x}}^2}\right). \tag{35}$$

We compare Algorithm 1 and 2 in terms of MSE in the estimation of time delays as:

$$\text{MSE} = 10\log\left(\sum_{\ell=1}^{L}(\tau_\ell - \hat{\tau}_\ell)^2\right). \tag{36}$$

For both the approaches, we used same number of firing rates and measurements. The time delays are estimated by OMP algorithm. The MSEs in the time delay estimation are shown in Fig. 9 for different SNRs and for $K = L, 2L$. We observe that for SNR> -20 dB, Algorithm 2 has lower error compared to Algorithm 1.

C. Numerical Results for Off-Grid Time-Delays

The following experiments consider off-grid time-delays with $h(t)$ as a third-order cubic B-spline. We consider $L = 3$ pulses where time-delays and amplitudes are generated uniformly at random over intervals $(0, T]$ and $[1, 5]$, respectively. For IF-TEM, we set $\kappa = 1$ and $b = 2.5c$ where c is computed as in (18). The threshold δ is chosen to satisfy (24). To compare the methods with zero and without-zero frequency, we consider sampling SoS kernels with $\mathcal{K} = \{-K, \ldots, K\}$ and $\{-K, \ldots, -1, 1, \ldots, K\}$, respectively. We use an annihilating filter with Cadzow denoising to estimate the time-delays in the presence of noise. Since Cadzow denoising requires more than $2L$ consecutive samples of FSCs, we consider $K \geq 2L + 1$ while excluding the zero. Based on the fact that Algorithm 2 estimates $\{\hat{x}[k]\}_{k=-K}^{-1}$ and $\{\hat{x}[k]\}_{k=1}^{K}$, we apply Cadzow denoising on each of these sequences independently and then apply block annihilation [32] to determine the time-delays jointly. In addition, we also show results for estimation of signal parameters via rotational invariance technique (ESPRIT) [33] for with zero approach.

In this simulation, we compare the two approaches in terms of MSEs (cf. (36)) when the time encodings are perturbed. The perturbed time encodings are given as $t'_n = t_n + \epsilon_n$ where t_n is the actual time encoding and ϵ_n is a random variable uniformly distributed over $[-\sigma/2, \sigma/2]$. The MSEs in the estimation of time-delays for different numbers of FSCs and perturbation levels are shown in Fig. 10. We used 500 independent noise and FRI signal realizations to compute each MSE value. In Fig. 10(a), (b), and (c) we show MSEs for with zero, without zero, and ESPRIT approaches. In Fig. 10(d), we show one-dimensional MSE plots for $K = 2L + 1$ and $5L$ for further clarity. In the present experimental settings, the time encodings have values between $[0, T]$ where $T = 1$ sec. In this case, adding a perturbation with $\sigma \geq 0.04$ has severe effect on the recovery with MSE in the range of -5 dB for all the approaches. We observe that the zero approach and ESPRIT have similar MSEs. While comparing these two approaches with the proposed without zero approach, we note a gain of $3 - 10$ dB for $\sigma < 0.04$. Since perturbation in the time encoding is also equivalent to quantization noise, a lower MSE indicates that the proposed without zero approach can operate at lower bits compared to with zero method.

D. Resolution and Firing Rate Analysis

The accuracy of time-delay estimations of any FRI recovery approach is strongly dependent on the minimum distance between two consecutive FRI pulses in the presence of noise. To analyze the resolution abilities of the two approaches, we consider an FRI signal with two pulses of equal amplitudes. By treating the difference between the time delays, $\tau_2 - \tau_1$, we computed MSEs (as in (36)) in their estimation when the time encodings are perturbed with $\sigma = 0.008$ (low noise) and $\sigma = 0.014$ (high noise). The results are shown in Fig. 11. For both the noise levels without zero approach has a lower MSE compared to the with zero approach. The gain in the MSE is more prominent (up to 5 dB) for the high noise level. The results shows that without zero approach has better resolution compared to the with zero approach.

Unlike conventional sampling, the number of measurements per unit time in the IF-TEM is not fixed. For a class of c-bounded FRI signals, we choose parameters $\{\kappa, b, \delta\}$ to achieve a desired minimum firing rate. However, the firing rate may vary from signal to signal in the class considered. Importantly, the bias

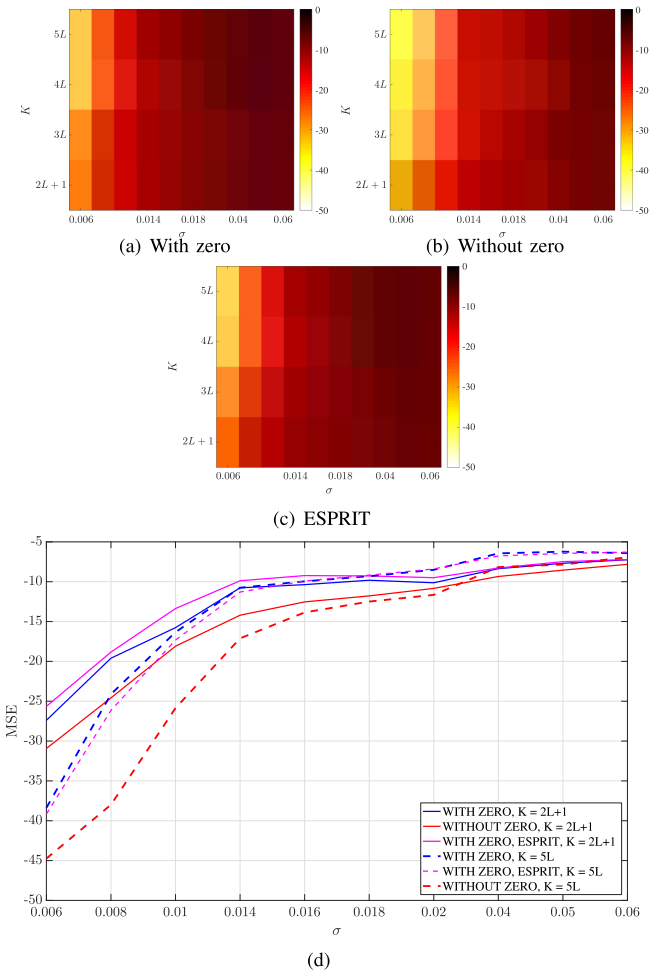

Fig. 10. A comparison of with zero (Algorithm 1) and without zero (Algorithm 2) approaches for off-grid time delays with perturbation in the time encodings: Without zero method has lower error compared to with zero approach.

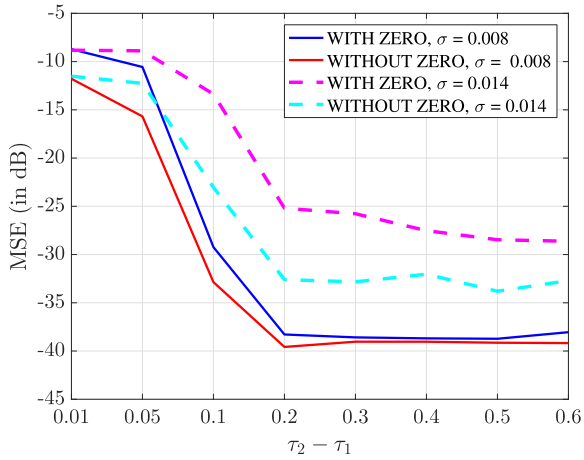

Fig. 11. Comparison of resolutions of the without zero (Algorithm 1) and without zero (Algorithm 2): Without zero approach has lower error compared to the with zero method.

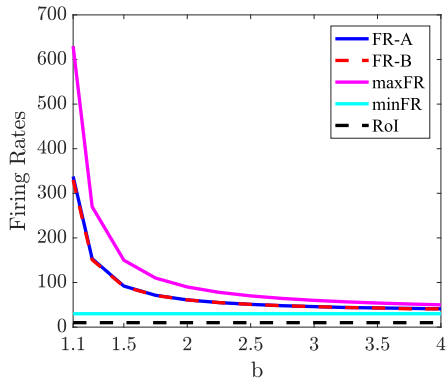

Fig. 12. Comparison of firing rates: FR-A and FR-B denotes mean firing rates of with zero and without zero approaches, respectively. Maximum and minimum rates are denoted by maxFR and minFR, respectively. As b increases, firing rates reach closer to RoI.

b plays a crucial role in designing the rate as it should always be kept above c. In this experiment, we analyze the effect of b on the firing rate for a fixed c. To this end, we set $c = 1$ and vary b. For each b, we generate 100 FRI signals with randomly chosen amplitudes and time-delays such that the signals are bounded by c. We compute the average firing rates for both with zero (denoted as FR-A) and without zero (denoted as FR-B) approaches as shown in Fig. 12. We also plotted the maximum firing (maxFR) and minimum firing (minFR) rates, $\frac{b+c}{\kappa\delta}$ and $\frac{b-c}{\kappa\delta}$ together with the rate of innovation (RoI) $2L$. Here we chose $L = 5$ and kept it fixed for all b. For each b, κ is set to be 1 and δ is selected to satisfy (24). For both methods, we have identical mean firing rates.

We observe that for small values of b, the firing rates are large, and they reduce as b increases. For large values of b, the gap between maxFR and min FR reduces, and IF-TEM operates at a rate closer to RoI. However, a large b amounts to high power consumption. Hence, there is a trade-off between power consumption and the optimum firing rate.

V. Reconstruction of Nonperiodic FRI Signals

Consider a nonperiodic FRI signal of the form

$$\tilde{x}(t) = \sum_{\ell=1}^{L} a_\ell h(t - \tau_\ell), \tag{37}$$

where $h(t)$ is a known pulse and the amplitudes and delays $\{(a_\ell, \tau_\ell) | \tau_\ell \in [0, T), a_\ell \in \mathbb{R}\}_{\ell=1}^{L}$ are unknown parameters. We assume that the pulse $h(t)$ has finite support R, namely

$$h(t) = 0, \quad \forall |t| \geq \frac{R}{2}. \tag{38}$$

Given that our main interest is in pulses with a very wide or even infinite spectrum, i.e very short pulses, traditional sampling techniques will prove to be ineffective in our case [22]. We design a sampling kernel $\tilde{g}(t)$ such that

$$\tilde{y}(t) = \tilde{x}(t) * \tilde{g}(t) = y(t), \quad \forall t \in [0, T), \tag{39}$$

where $y(t)$ defined in (11). Specifically, $\tilde{g}(t)$ is compactly supported and defined by

$$\tilde{g}(t) = \sum_{s=-S}^{S} g(t + sT), \tag{40}$$

where S is determined by R and T (More details are available in [22]). Since both time instants and the time delays of the FRI signals are within the interval $[0, T)$, i.e., $t_n \in [0, T)$ and $\tau_\ell \in [0, T)$, $\ell = 1, \ldots, L$, the time instants taken in the nonperiodic case using IF-TEM are the same as in the periodic case. Therefore, the recovery guarantees developed for the periodic

$$\mathbf{V} = \begin{pmatrix} e^{-jK\omega_0 t_1} & \dots & e^{-j\omega_0 t_1} & t_1 & e^{j\omega_0 t_1} & \dots & e^{jK\omega_0 t_1} \\ e^{-jK\omega_0 t_2} & \dots & e^{-j\omega_0 t_2} & t_2 & e^{j\omega_0 t_2} & \dots & e^{jK\omega_0 t_2} \\ \vdots & \ddots & \vdots & \vdots & \vdots & \ddots & \vdots \\ e^{-jK\omega_0 t_N} & \dots & e^{-j\omega_0 t_N} & t_N & e^{j\omega_0 t_N} & \dots & e^{jK\omega_0 t_N} \end{pmatrix} \in \mathbb{C}^{N\times 2K+1} \tag{43}$$

$$\underbrace{\begin{pmatrix} e^{-jK\omega_0 t_1} & \dots & e^{-j\omega_0 t_1} & 1 & e^{j\omega_0 t_1} & \dots & e^{jK\omega_0 t_1} \\ e^{-jK\omega_0 t_2} & \dots & e^{-j\omega_0 t_2} & 1 & e^{j\omega_0 t_2} & \dots & e^{jK\omega_0 t_2} \\ \vdots & \ddots & \vdots & \vdots & \vdots & \ddots & \vdots \\ e^{-jK\omega_0 t_N} & \dots & e^{-j\omega_0 t_N} & 1 & e^{j\omega_0 t_N} & \dots & e^{jK\omega_0 t_N} \end{pmatrix}}_{\mathbf{W}} \underbrace{\begin{pmatrix} \bar{x}[-K] \\ \vdots \\ \bar{x}[-1] \\ -c \\ \bar{x}[1] \\ \vdots \\ \bar{x}[K] \end{pmatrix}}_{\bar{\mathbf{x}}} = -\bar{x}[0] \underbrace{\begin{pmatrix} t_1 \\ t_2 \\ \vdots \\ t_N \end{pmatrix}}_{\mathbf{t}} \tag{44}$$

case in Theorems 4 and 2 are applicable to the non-periodic case as well.

VI. Conclusion

In this paper, we consider sampling and reconstruction frameworks for periodic FRI signals by using IF-TEMs. We first provide theoretical guarantees for the approach provided in [12]. We then propose a robust recovery approach by modifying the sampling kernel. We show that in the presence of perturbations of time encodings, the modified approach outperforms the method in [12] for the same number of measurements. Compared to conventional amplitude-based sampling for FRI signals the proposed TEM-based method is less power consuming and hence, more cost effective.

Appendix

In this Appendix we prove Theorems 1 and 3. We consider a unified approach to prove both the theorems by using the fact that the proof of Theorem 3 is a special case of that of Theorem 1 with $\hat{x}[0] = 0$.

Proof: The matrix $\mathbf{A}$ in (22) is decomposed as

$$\mathbf{A} = \mathbf{D}\mathbf{V}, \tag{41}$$

where

$$\mathbf{D} = \begin{pmatrix} -1 & 1 & 0 & \cdots & 0 \\ 0 & -1 & 1 & \cdots & 0 \\ 0 & 0 & -1 & \cdots & 0 \\ \vdots & \vdots & \vdots & \ddots & \vdots \\ 0 & 0 & 0 & \cdots & 1 \end{pmatrix} \in \mathbb{R}^{(N-1)\times N} \tag{42}$$

and $\mathbf{V}$ is given as in (43). To determine $\hat{\mathbf{x}}$ uniquely from $\mathbf{y} = \mathbf{D}\mathbf{V}\hat{\mathbf{x}}$, the matrix $\mathbf{A}$ should not have a non-zero null space vector.

The matrix $\mathbf{D}$ is a difference operator which has null space vector $c\mathbf{1}_N$ where $c \in \mathbb{C}\backslash\{0\}$. Hence, if there exist a non-zero vector $\mathbf{x}$ as in (21) whose components satisfy (9), such that $\mathbf{V}\mathbf{x} = c\mathbf{1}_N$ for some arbitrary c, then there does not exist a unique solution. We show that for $N \geq 2K+2 \geq 2L+1$, uniqueness is guaranteed. Specifically, we would like to show that there does not exist an $\mathbf{x}$ satisfying (9), a set $\{t_n\}_{n=1}^N$, and $c \neq 0$ such that $\mathbf{V}\mathbf{x} = c\mathbf{1}_N$ for $N > 2K+1$ (43) and (44) are shown at top of this page.

For simplicity of discussion, we define $\bar{x}[k] = \frac{\hat{x}[k]}{jk\omega_0}$ for $k \neq 0$ and $\bar{x}[0] = \hat{x}[0]$. The modulus and angle of the complex-valued coefficient $x[k]$ is denoted by $|x[k]|$ and $\angle x[k]$, respectively. The equation $\mathbf{V}\mathbf{x} = c\mathbf{1}_N$ is re-written as in (44) or alternatively as

$$f(t) = r(t), \quad \text{for} \quad t = t_1, \dots, t_N, \tag{45}$$

where

$$f(t) = c - 2\sum_{k=1}^{K} |\bar{x}[k]| \cos(k\omega_0 t + \angle \bar{x}[k]) \tag{46}$$

is a K-th order trigonometric polynomial and $r(t) = \bar{x}[0]t$ is a straight line with slope $\bar{x}[0]$. If there exist a c and $\{\bar{x}[k]\}_{k=0}^K$ such that $f(t)$ and $r(t)$ intersect each other N-times within an interval $[0, T)$, that is, there exists a set $\mathcal{T}_N = \{t_n \in [0, T), n = 1, \dots, N\}$ satisfying $f(t) = r(t)$ then uniqueness is not guaranteed.

Let us consider two mutually exclusive cases: (1) $\bar{x}[0] = \hat{x}[0] = 0$ and (2) $\bar{x}[0] = \hat{x}[0] \neq 0$.

Case-1: For $\bar{x}[0] = 0$, the slope of the straight line $r(t)$ is zero and hence, (45) is equivalent to determining zeros of $f(t)$ in the interval $[0, T)$. Since $f(t)$ is a trigonometric polynomial of order K with $\omega_0 = \frac{2\pi}{T}$, it will have a maximum of $2K$ zeros within the interval $[0, T)$ [34, p. 150]. Hence, for $N > 2K$, there does not exist a $c \neq 0$ and a feasible $\{\bar{x}[k]\}_{k=0}^K$ such that (45) holds true.

Case-2: Consider the case when $\bar{x}[0] \neq 0$. We intend to determine the maximum number of intersections of a trigonometric polynomial of order K with a straight line. To this end, let t_1 be the first intersection point. Further, let us assume that the slope of $f(t)$ at $t = t_1$ is positive (or negative), that is, $f'(t_1) > 0$ (or $f'(t_1) < 0$) where $f'(t)$ denotes derivative of $f(t)$. This implies that there may exist a minimum (or maximum) of $f(t)$ for $t \in [0, t_1)$ and a maximum (or minimum) for $t \in (t_1, T)$. An

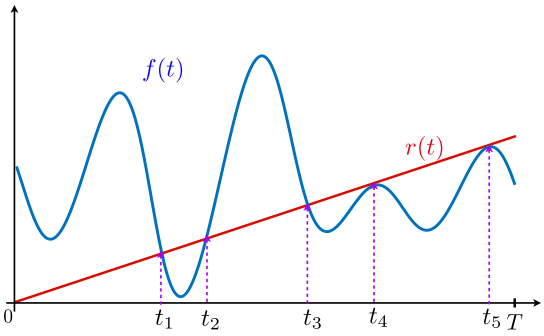

Fig. 13. An illustration of intersection of a trigonometric polynomial $f(t)$ and a straight line $r(t)$.

illustrative example is shown in Fig. 13. Since $r(t)$ is a monotone function, to have a second intersection t_2, it is necessary that $f'(t)$ changes its sign. In essence, if there exist a $t_2 \in \mathcal{T}_N$, then there should be a maximum (or minimum) of $f(t)$ in the interval (t_1, t_2). Applying this argument to the remaining intersection points in $\mathcal{T}_N$ we infer that for N intersection points there should be atleast $N-1$ extrema. Alternatively, a function with $N-1$ extrema can intersect a monotone function at a maximum of N points. As $f'(t)$ too is a K-th order trigonometric polynomial, it has a maximum of $2K$ zeros [34, p. 150]. This implies that $f(t)$ can have a maximum of $2K$ extrema. Hence, $f(t)$ can intersect $r(t)$ at a maximum of $2K+1$ points within interval $[0, T)$. This implies that for $N > 2K+1$, the equation $f(t) = r(t)$ can not have any solution and hence, matrix $\mathbf{A}$ does not have a non-zero null-vector and uniqueness is guaranteed. □

REFERENCES

[1] Y. C. Eldar, *Sampling Theory: Beyond Bandlimited Systems*. New York, NY, USA: Cambridge Univ. Press, 2015.

[2] M. Unser, "Sampling-50 years after Shannon," *Proc. IEEE*, vol. 88, no. 4, pp. 569–587, Apr. 2000.

[3] H. Nyquist, "Certain topics in telegraph transmission theory," *Trans. Amer. Inst. Elect. Eng.*, vol. 47, no. 2, pp. 617–644, 1928.

[4] Y. C. Eldar, "Compressed sensing of analog signals in shift-invariant spaces," *IEEE Trans. Signal Process.*, vol. 57, no. 8, pp. 2986–2997, Aug. 2009.

[5] O. Christensen and Y. C. Eldar, "Oblique dual frames and shift-invariant spaces," *Appl. Comput. Harmon. Anal.*, vol. 17, no. 1, pp. 48–68, 2004.

[6] M. Malmirchegini, M. M. Kafashan, M. Ghassemian, and F. Marvasti, "Non-uniform sampling based on an adaptive level-crossing scheme," *IET Signal Process.*, vol. 9, pp. 484–490, Aug. 2015.

[7] A. A. Lazar and L. T. Tóth, "Perfect recovery and sensitivity analysis of time encoded bandlimited signals," *IEEE Trans. Circuits Syst. I: Reg. Papers*, vol. 51, no. 10, pp. 2060–2073, Oct. 2004.

[8] K. Adam, A. Scholefield, and M. Vetterli, "Sampling and reconstruction of bandlimited signals with multi-channel time encoding," *IEEE Tran. Signal Process.*, vol. 68, pp. 1105–1119, Jan. 2020, doi: 10.1109/TSP.2020.2967182.

[9] M. Rastogi, V. Garg, and J. G. Harris, "Low power integrate and fire circuit for data conversion," in *Proc. IEEE Int. Symp. Circuits Syst.*, 2009, pp. 2669–2672.

[10] R. Alexandru and P. L. Dragotti, "Reconstructing classes of non-bandlimited signals from time encoded information," *IEEE Trans. Signal Process.*, vol. 68, pp. 747–763, Dec. 2019, doi: 10.1109/TSP.2019.2961301.

[11] M. Hilton, R. Alexandru, and P. L. Dragotti, "Time encoding using the hyperbolic secant kernel," in *Proc. IEEE Eur. Signal Process. Conf.*, 2021, pp. 2304–2308.

[12] S. Rudresh, A. J. Kamath, and C. S. Seelamantula, "A time-based sampling framework for finite-rate-of-innovation signals," in *Proc. IEEE Int. Conf. Acoust. Speech Signal Process.*, 2020, pp. 5585–5589.

[13] K. Adam, A. Scholefield, and M. Vetterli, "Encoding and decoding mixed bandlimited signals using spiking integrate-and-fire neurons," in *Proc. IEEE Int. Conf. Acoust. Speech Signal Process.*, 2020, pp. 9264–9268.

[14] P. Martínez-Nuevo, H.-Y. Lai, and A. V. Oppenheim, "Delta-ramp encoder for amplitude sampling and its interpretation as time encoding," *IEEE Trans. Signal Process.*, vol. 67, no. 10, pp. 2516–2527, May 2019.

[15] B. Rajendran, A. Sebastian, M. Schmuker, N. Srinivasa, and E. Eleftheriou, "Low-power neuromorphic hardware for signal processing applications: A review of architectural and system-level design approaches," *IEEE Signal Process. Mag.*, vol. 36, no. 6, pp. 97–110, Nov. 2019.

[16] F. Barranco, C. Fermüller, and Y. Aloimonos, "Contour motion estimation for asynchronous event-driven cameras," *Proc. IEEE*, vol. 102, no. 10, pp. 1537–1556, Oct. 2014.

[17] A. A. Lazar, "Time encoding with an integrate-and-fire neuron with a refractory period," *Neurocomputing*, vol. 58, pp. 53–58, 2004.

[18] A. A. Lazar and L. T. Tóth, "Time encoding and perfect recovery of bandlimited signals," in *Proc. IEEE Int. Conf. Acoust. Speech Signal Process.*, 2003, pp. VI–709.

[19] H. G. Feichtinger, J. C. Príncipe, J. L. Romero, A. S. Alvarado, and G. A. Velasco, "Approximate reconstruction of bandlimited functions for the integrate and fire sampler," *Adv. Comput. Math.*, vol. 36, no. 1, pp. 67–78, 2012.

[20] K. Adam, A. Scholefield, and M. Vetterli, "Multi-channel time encoding for improved reconstruction of bandlimited signals," in *Proc. IEEE Int. Conf. Acoust. Speech Signal Process.*, 2019, pp. 7963–7967.

[21] M. Vetterli, P. Marziliano, and T. Blu, "Sampling signals with finite rate of innovation," *IEEE Trans. Signal Process.*, vol. 50, no. 6, pp. 1417–1428, Jun. 2002.

[22] R. Tur, Y. C. Eldar, and Z. Friedman, "Innovation rate sampling of pulse streams with application to ultrasound imaging," *IEEE Trans. Signal Process.*, vol. 59, no. 4, pp. 1827–1842, Apr. 2011.

[23] J. A. Urigüen, Y. C. Eldar, P. L. Dragotti, and Z. Ben-Haim, "Sampling at the rate of innovation: Theory and applications," in *Compressed Sensing: Theory and Applications*, Cambridge, U.K.: Cambridge Univ. Press, 2012, pp. 148–209.

[24] O. Bar-Ilan and Y. C. Eldar, "Sub-Nyquist radar via doppler focusing," *IEEE Trans. Signal Process.*, vol. 62, no. 7, pp. 1796–1811, Apr. 2014.

[25] W. U. Bajwa, K. Gedalyahu, and Y. C. Eldar, "Identification of parametric underspread linear systems and super-resolution radar," *IEEE Trans. Signal Process.*, vol. 59, no. 6, pp. 2548–2561, Jun. 2011.

[26] S. Rudresh and C. S. Seelamantula, "Finite-rate-of-innovation-sampling-based super-resolution radar imaging," *IEEE Trans. Signal Process.*, vol. 65, no. 19, pp. 5021–5033, Oct. 2017.

[27] S. Mulleti, S. Nagesh, R. Langoju, A. Patil, and C. S. Seelamantula, "Ultrasound image reconstruction using the finite-rate-of-innovation principle," in *Proc. IEEE Int. Conf. Image Process.*, 2014, pp. 1728–1732.

[28] S. Mulleti, B. A. Shenoy, and C. S. Seelamantula, "FRI sampling on structured nonuniform grids-application to super-resolved optical imaging," *IEEE Trans. Signal Process.*, vol. 64, no. 15, pp. 3841–3853, Aug. 2016.

[29] D. L. Donoho, "Compressed sensing," *IEEE Trans. Inf. Theory*, vol. 52, no. 4, pp. 1289–1306, Apr. 2006.

[30] P. Stoica and R. L. Moses, *Introduction to Spectral Analysis*. Englewood Cliffs, NJ, USA: Prentice Hall, 1997.

[31] D. Gontier and M. Vetterli, "Sampling based on timing: Time encoding machines on shift-invariant subspaces," *Appl. Comput. Harmon. Anal.*, vol. 36, no. 1, pp. 63–78, 2014.

[32] Y. Barbotin, A. Hormati, S. Rangan, and M. Vetterli, "Estimation of sparse MIMO channels with common support," *IEEE Trans. Commun.*, vol. 60, no. 12, pp. 3705–3716, Dec. 2012.

[33] R. Roy and T. Kailath, "ESPRIT-estimation of signal parameters via rotational invariance techniques," *IEEE Trans. Acoust., Speech, Signal Process.*, vol. 37, no. 7, pp. 984–995, Jul. 1989.

[34] M. J. D. Powell, *Approximation Theory and Methods*. New York, NY, USA: Cambridge Univ. Press, 1981.

Hila Naaman (Student Member, IEEE) received the B.Sc. degree in physics and mathematics from Bar-Ilan university, Ramat Gan, Isreal, in 2012, and the M.Sc. degree in physics in 2017. She is currently working toward the Doctoral degree with the Mathematics and Computer Science Department, Weizmann Institute of Science, Rehovot, Israel, under the supervision of Prof. Yonina C. Eldar. Her research interests include event-based information processing, signal processing, sampling theory and its applications.

Satish Mulleti (Member, IEEE) received the B.Eng. degree from the Electronics and Communication Engineering Department, Jalpaiguri Government Engineering College, Jalpaiguri, India, in 2005, and the M.Eng. degree in electrical engineering from the Department of Electrical Engineering, Indian Institute of Technology Kanpur, Kanpur, India, in 2009. He was a Researcher with the Indian Space Research Organization (ISRO), India and Tata Consultancy Services (TCS) Innovation Laboratories, Mumbai, India. In August 2011, he joined the Spectrum Laboratory, Department of Electrical Engineering, Indian Institute of Science, Bangalore, Bangalore, India, for his Ph.D. degree. From April 2017 to August 2021, he was a Postdoc with the Department of Electrical Engineering, Technion - Israel Institute of Technology, Haifa, Israel, and Mathematics and Computer Science Department, Weizmann Institute of Science, Rehovot, Israel. He is currently an Assistant Professor with the Department of Electrical Engineering, Indian Institute of Technology (IIT) Bombay, India. His research interests include sampling theory, in particular, finite-rate-of-innovation signal sampling, compressive sensing, machine learning, blind deconvolution, sparse array signal processing, and spectral estimation.

Yonina C. Eldar (Fellow, IEEE) received the B.Sc. degree in physics and the B.Sc. degree in electrical engineering both from Tel-Aviv University, Tel-Aviv, Israel, in 1995 and 1996, respectively, and the Ph.D. degree in electrical engineering and computer science from the Massachusetts Institute of Technology, Cambridge, MA, USA, in 2002. She is currently a Professor with the Department of Mathematics and Computer Science, Weizmann Institute of Science, Rehovot, Israel. She was a Professor with the Department of Electrical Engineering, Technion, where she held the Edwards Chair in Engineering. She is also a Visiting Professor with MIT, a Visiting Scientist with the Broad Institute, Cambridge, MA, USA, and an Adjunct Professor with Duke University, Durham, NC, USA, and was a Visiting Professor with Stanford University, Stanford, CA, USA. She is a Member of the Israel Academy of Sciences Joint Transmit Beamforming for Multiuser MIMO Communications and MIMO Radar 17 and Humanities (elected 2017) and a EURASIP Fellow. Her research interests include statistical signal processing, sampling theory and compressed sensing, learning and optimization methods, and their applications to biology and optics. She was the recipient of many awards for excellence in research and teaching, including the IEEE Signal Processing Society Technical Achievement Award (2013), the IEEE/AESS Fred Nathanson Memorial Radar Award (2014), and the IEEE Kiyo Tomiyasu Award (2016). She was a Horev Fellow of the Leaders in Science and Technology program with the Technion, Haifa, Israel, and an Alon Fellow. She also was the recipient of the Michael Bruno Memorial Award from the Rothschild Foundation, the Weizmann Prize for Exact Sciences, the Wolf Foundation Krill Prize for Excellence in Scientific Research, the Henry Taub Prize for Excellence in Research (twice), the Hershel Rich Innovation Award (three times), the Award for Women with Distinguished Contributions, the Andre and Bella Meyer Lectureship, the Career Development Chair with the Technion, the Muriel & David Jacknow Award for Excellence in Teaching, and the Technion's Award for Excellence in Teaching (two times), several best paper awards and best demo awards together with her research students and colleagues, including the SIAM outstanding Paper Prize, the UFFC Outstanding Paper Award, the Signal Processing Society Best Paper Award and the IET Circuits, Devices and Systems Premium Award, and was selected as one of the 50 most influential women in Israel. She was a Member of the Young Israel Academy of Science and Humanities and the Israel Committee for Higher Education. She is the Editor-in-Chief for *Foundations and Trends in Signal Processing*, a Member of the IEEE Sensor Array and Multichannel Technical Committee and serves on several other IEEE committees. In the past, she was a Signal Processing Society Distinguished Lecturer, a Member of the IEEE SIGNAL PROCESSING THEORY AND METHODS and Bio Imaging Signal Processing technical committees, and was an Associate Editor for the IEEE TRANSACTIONS ON SIGNAL PROCESSING, the *EURASIP Journal of Signal Processing*, the *SIAM Journal on Matrix Analysis and Applications*, and the *SIAM Journal on Imaging Sciences*. She was the Co-Chair and Technical Co-Chair of several international conferences and workshops.